International Journal of Heat and Mass Transfer 52 (2009) 1472–1480

Contents lists available at ScienceDirect

International Journal of Heat and Mass Transfer

journal homepage: www.elsevier.com/locate/ijhmt

On the bubble departure diameter and release frequency based on numerical simulation results

Gabor Hazi *, Attila Markus

MTA KFKI Atomic Energy Research Institute, Theoretical Thermohydraulics Research Group, H-1525 Budapest, Hungary

ARTICLE INFO

Article history:
Received 18 July 2008
Available online 12 November 2008

Keywords:
Nucleate boiling
Bubble departure diameter
Bubble release frequency
Lattice Boltzmann method

ABSTRACT

Heterogeneous boiling on a horizontal plate in stagnant and slowly flowing fluid is simulated using the lattice Boltzmann approach. The bubble departure diameter and release frequency are determined from the simulation results. It is found that the bubble departure diameter is proportional to $g^{-1/2}$ in a stagnant fluid and the release frequency scales with $g^{3/4}$, where g is the gravitational acceleration. Simulation results show no dependence between the bubble departure diameter and the static contact angle, but the bubble release frequency increases exponentially with the latter. Considering forced boiling, exponential relation is observed between the bubble departure diameter and the flow driving pressure gradient.

1. Introduction

Departure from nucleate boiling (DNB) is the main governing critical heat flux mechanism in pressurized water nuclear reactors. According to Bestion et al. [3] the phenomenology of convective boiling and DNB is very complex and many of small scale processes, which finally lead to DNB (activation of nucleation sites, growing of attached bubbles, detachment of the bubbles, etc.) are not well understood. Thus, detailed investigation of those processes is needed to improve our understanding and the predictive capabilities of large scale industrial two-phase flow simulation tools. According to Dhir's recent review [9], despite substantial efforts made in the last 70 years, we do not yet have a comprehensive model for the subprocesses build up a global nucleate boiling process. In this work one of those subprocesses, namely the bubble departure is analyzed based on numerical simulation results. To be more specific, we study the bubble departure diameter and release frequency, two key quantities in the puzzle of determining the nucleate boiling heat flux. A bubble attaching, growing on and departing from a heated wall have been studied very intensively using analytical [12,6], numerical [1,4,10,11,13,14,24,27,29,31–34,39,40,47] and measurement [28,8,2,46,23,41] techniques. Considering the numerical approach, several models have been developed to study the growing process. Many of these models divide the geometrical domain into parts around a growing bubble using different transfer models for the so-called micro- and macro-regions (see e.g. [11]) or simplify the problem, assuming for instance, saturated liquid at the bubble dome [31]. Beside these approximations, the liquid–vapor interface has usually been tracked by some level-set method (see e.g. [11]). In the present work, a new method is proposed to simulate nucleate boiling without using any of the above-mentioned simplifications. The method is based on the pseudo-potential extension of the lattice Boltzmann equation and it is extended with an energy transfer equation to model heat transfer. The wettability of the heated wall is modeled by an interaction force between the solid wall and the fluid. Using this method, growing bubble on a heated surface is simulated both in stagnant and slowly flowing fluid. The diameter of the bubble at departure and the bubble release frequency are determined from the simulation results. Relations between these quantities and gravity, fluid velocity, wettability are established based on the numerical data.

2. The lattice Boltzmann method

2.1. Mass and momentum conservation equations

The lattice Boltzmann method (LBM) is an innovative technique for modeling two-phase flows. Many different models have been developed in the framework of LBM to model bubbly flows see e.g. [36,37,21,22,26], or [43]. In this work the multiphase model of Shan and Chen was adopted [38] and extended to model heterogeneous boiling. For completeness, here we give a brief review on the base method. To model multiphase flows, Shan and Chen proposed [38] to solve the lattice Boltzmann equation with Bhatnagar–Gross–Krook collision operator [5]

$$f_i(\mathbf{x}+\mathbf{c}_i\Delta t, t+\Delta t) - f_i(\mathbf{x},t) = -\frac{1}{\tau}\left(f_i - f_i^{\mathrm{eq}}\right), \tag{1}$$

* Corresponding author.
E-mail addresses: gah@aeki.kfki.hu (G. Hazi), amarkus@aeki.kfki.hu (A. Markus).

0017-9310/$ - see front matter © 2008 Elsevier Ltd. All rights reserved.
doi:10.1016/j.ijheatmasstransfer.2008.09.003

where $f_i(\mathbf{x},t)$ is the one-particle velocity distribution function, $\mathbf{c}_i$ is the lattice velocity vector, τ is the relaxation time which controls the rate of approach to the local equilibrium $f_i^{eq}(\mathbf{x},t)$ and Δt is the timestep.

The local equilibrium distribution is written as

$$f_i^{eq} = w_i\rho\left[1 + 3c_{i\alpha}u_\alpha^{eq} - \frac{3}{2}u_\alpha^{eq}u_\alpha^{eq} + \frac{9}{2}c_{i\alpha}c_{i\beta}u_\alpha^{eq}u_\beta^{eq}\right], \tag{2}$$

which is a low Mach number expansion of the Maxwell–Boltzmann distribution.

For the calculations presented in this paper we used a two-dimensional nine-velocity (D2Q9) model, for which the lattice velocity vectors $\mathbf{c}_i$ and weights w_i are defined by

$$\mathbf{c}_i = \begin{cases} (0,0) & i=0, \\ (\pm1,0),(0,\pm1) & i=1.4,, \\ (\pm1,\pm1) & i=5.8 \end{cases} \quad w_i = \begin{cases} 4/9 & i=0, \\ 1/9 & i=1.4, \\ 1/36 & i=5.8. \end{cases} \tag{3}$$

The density and hydrodynamic velocity of the fluid are given as follows:

$$\rho = \sum_i f_i, u_\alpha\rho = u'_\alpha\rho + 1/2\Delta t F_\alpha, \tag{4}$$

where

$$u'_\alpha = \sum_i c_{i\alpha}f_i, \tag{5}$$

and the force F_α will be defined later on. The velocity used in the equilibrium distribution function (2) is calculated from

$$u_\alpha^{eq} = u'_\alpha + \frac{\tau}{\rho}F_\alpha. \tag{6}$$

It can be shown that the mesoscopic evolution of the particle distribution functions (1), yields the macroscopic equations [7]

$$\partial_t\rho + \partial_\beta(\rho u_\beta) = 0, \tag{7}$$

$$\partial_t u_\alpha + u_\beta\partial_\beta u_\alpha + \frac{1}{\rho}\left[\partial_\alpha\left(\frac{\rho}{3}\right) - F_\alpha\right] = \nu\partial_\beta^2 u_\alpha, \tag{8}$$

with some error terms, which can be neglected at low Mach numbers or can be partially compensated at higher velocities [16].

That is we solve the Navier–Stokes equations in which the viscosity is given by

$$\nu = c_s^2\Delta\left(\tau - \frac{1}{2}\right), \tag{9}$$

and the force F_α determines the equation of state of the fluid.

2.2. Equation of state, binodal and surface tension

In order to model non-ideal gases and surface tension we need to choose a proper form for F_α. Shan and Chen proposed to calculate the force as the gradient of a particle interaction potential ψ [38]. In this work the same methodology was used, but a new form for the interaction potential was implemented:

$$\psi = \frac{\rho}{T + C_1\rho}. \tag{10}$$

Analytical results show that using this potential, Maxwell equal area construction, a requirement for thermodynamic consistency, can be satisfied in case of a flat liquid–vapor interface [17]. In (10) the parameter T plays the role of temperature and C_1 is a parameter, which can be used to control the surface tension.

The interaction force is calculated as the gradient of the pseudo-potential, which can be approximated in the lattice Boltzmann framework as

$$F_\alpha = -\psi(\mathbf{x})\sum_i w_i\psi(\mathbf{x}+\mathbf{c}_i)\mathbf{c}_i. \tag{11}$$

Using the above form of the force a fluid with the equation of state

$$p = \frac{1}{3}\left(\rho + \frac{1}{2}\psi^2\right) \tag{12}$$

can be modeled. As a straightforward demonstration of this fact one can set the initial density of the fluid between the spinodals of a given temperature and then phases must separate from each other by spinodal decomposition as far as a small amount of temperature or density noise is present, since the fluid is in the region $\left(\frac{\partial\rho}{\partial p} < 0\right)$. Depending on the initial conditions, the final state of such simulations is a flat interface which separates the individual phases or a spherical object (bubble or drop) surrounding by the complementer phase. After separation and the formation of a flat interface the phase densities correspond to the coexistence curve or binodal. The pressure is the same in the bulk phases and Maxwell's equal area construction is satisfied if the model is thermodynamically consistent. For the present model, the coexistence curve is shown in Fig. 1, where symbols represent simulation results and the solid line is calculated from the equation of state in accordance with Maxwell's equal area construction. Obviously, the agreement is excellent, as it expected from our analytical calculations [17].

The critical density and temperature of the fluid modeled can be calculated from the equations of state and they are given as

$$\rho_c = -\frac{2G}{27C_1^2}, \quad T_c = -\frac{4G}{27C_1}.$$

Throughout this paper we will use these critical values to have non-dimensional temperature and density. Mass, spatial and temporal dependent quantities are made non-dimensional dividing by one mass, lattice or timestep units, respectively. Although it is not given explicitly (see Eq. (8)), this model also represents surface tension. Actually, it is a consequence of the numerical approximation of the potential gradient as it can be shown by Taylor expanding the interaction force. However, instead of tedious analytical calculations we can calculate the surface tension in a straightforward manner using the results of numerical simulations. Setting up a low density circular region surrounded by a high density region at the center of a double periodic domain, the system evolves to a stable state. When the densities are near the binodals of an isotherm and the initial "bubble" diameter exceeds the critical radius [42] a stable bubble is formed in steady state. At this stage the surface tension can be determined from the pressure difference between the liquid and gas phases and from the bubble diameter according to Laplace's law. Surface tensions calculated in this way at different temperatures are shown in Fig. 2.

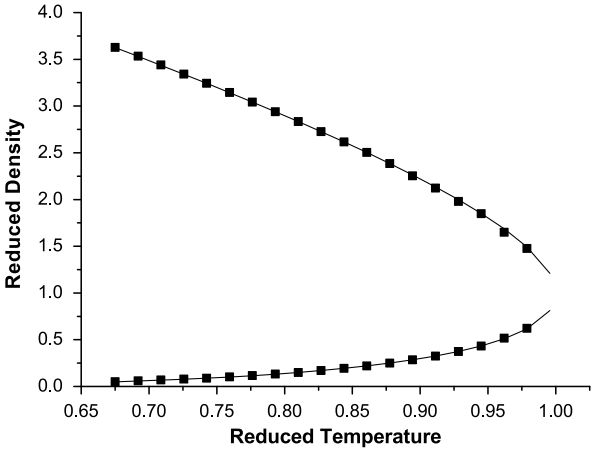

Fig. 1. Coexistence curve or binodal for the fluid modeled.

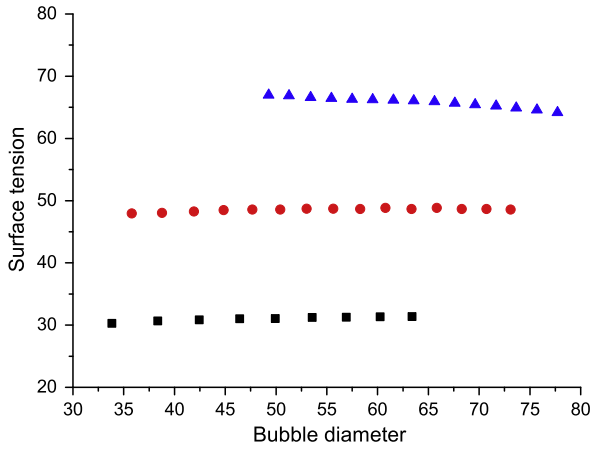

Fig. 2. Dimensionless surface tension for the fluid modeled at various temperatures (triangle – $T = 0.748$, circle – $T = 0.8$, and square – $T = 0.88$).

It is worth noting that Fig. 2 shows also the temperature dependency of the surface tension and that the latter has a weak linear relation with the bubble radius as one expects.

2.3. Energy equation

The method presented before can be used to model isothermal two-phase flow problems and introducing thermodynamic fluctuations, the method is also able to simulate homogenous nucleation [35,18]. To model such processes we need to initiate the system in a stable state (saturated liquid) and the thermodynamic fluctuations need to be high enough to drive the system locally into the metastable region. Then phase transition can occur. Note, however, that the metastable state is between the spinodals, so the fluctuations must high enough to achieve this region. Therefore, in order to model boiling in a real fluid, like water by this method we need a specific equation of state (modified between the binodals) and we need a corresponding potential given in analytical form. The development of such potential is in progress and results obtained for water will be published in the future. Here we limit the scope of our discussion to a model fluid defined by the equation of state (12). Considering heterogeneous boiling the model has to be supplemented by a transport equation for energy. There are two basic approaches to model thermal problems by the lattice Boltzmann method. Using the first approach one introduces energy conservation in mesoscopic level, defining the energy as the second moment of the distribution functions. Although this is a very attractive approach, all attempts before shown limited modeling capabilities because of numerical stability problems. It is worth noting that increasing the number of lattice links the stability of thermal models can be improved but this strategy leads to unacceptable computational demand considering the simulation of practical problems. Therefore, here we follow the second approach and make a thermal coupling in macroscopic level. It means that we define a second set of distribution functions g_i, which evolves according to the lattice Boltzmann equation

$$g_i(\mathbf{x}+\mathbf{c}_i\Delta t, t+\Delta t) - g_i(\mathbf{x}, t) = -\frac{1}{\kappa}\left(g_i - g_i^{\mathrm{eq}}\right) - w_i \Delta t q, \tag{13}$$

where the equilibrium distribution is given as follows:

$$g_i^{\mathrm{eq}} = w_i[T + 3c_{i\alpha}(Tu_\alpha - D_{\mathrm{T}}\partial_\alpha T)]. \tag{14}$$

We define the temperature as the following moment:

$$T = \sum_i g_i. \tag{15}$$

Performing a Chapman–Enskog expansion it can be shown [19] that the above evolution equation leads to the solution of the macroscopic equation

$$\partial_t T + \partial_\alpha(u_\alpha T) = \partial_\alpha\left(\widetilde{D}_{\mathrm{T}}\partial_\alpha T\right) - q, \tag{16}$$

where the thermal diffusion coefficient at constant volume is given by

$$\widetilde{D}_{\mathrm{T}} \equiv \frac{k}{\rho c_{\mathrm{v}}} = D_{\mathrm{T}} + \frac{\Delta t}{3}\left(\kappa - \frac{1}{2}\right). \tag{17}$$

Here k is the thermal conductivity and c_{v} is the specific heat at constant volume.

Now we need to specify the term q, which represents the energy change due to vaporization. This term is approximated by (see Appendix A for derivation)

$$q = -\frac{GT}{\rho c_{\mathrm{v}}}\gamma\frac{1}{\rho(T + C_1\rho^2)^3}, \tag{18}$$

where γ is the rate of vaporization

$$\gamma = \frac{\mathrm{d}\rho}{\mathrm{d}t}. \tag{19}$$

2.4. Model for static contact angle

Introducing interactions between the fluid and a solid wall, the wettability of the surface by the fluid can be modeled, too [30]. The interaction force is defined as

$$F_\alpha = -G_{\mathrm{w}}\psi(\mathbf{x})\sum_i w_i s(\mathbf{x}+\mathbf{c}_i)\mathbf{c}_i, \tag{20}$$

where $s(\mathbf{x}+\mathbf{c}_i)$ is a binary function (=1 for solid and =0 for fluid nodes).

The parameter G_{w} controls the strength of the intermolecular force between wall and fluid and therefore it can influence the wettability of the wall. In macroscopic level the static contact angle is used to parameterize the wettability. Therefore, to make a relation between mesoscopic and macroscopic parameters, simulations have been carried out by varying G_{w} and studying its effect on the wettability. The simulation domain was a rectangular domain with periodic boundaries on its left and right boundaries. Non-slip wall was modeled at the bottom and constant equilibrium pressure was specified at the top of the domain. The initial density field was set up to mimic the half of a bubble at the bottom plate (initial densities corresponded to the gas and liquid branches of the coexistence curve). Depending on the parameter G_{w}, the equilibrium profiles were different at the end of the simulations. In Fig. 3 the shapes of the attached bubbles are shown as the outcome of these simulations. These contours can be used to measure the static contact angle. Based on these simulations a linear relation could be deduced between G_{w} and the static contact angle (see e.g. $G_{\mathrm{w}} = -0.06$, $G_{\mathrm{w}} = -0.12$ and $G_{\mathrm{w}} = -0.18$ correspond to the contact angle 60°, 90° and 120°, respectively).

2.5. Boundary conditions

For the simulation of heterogeneous boiling we used a rectangular domain periodic in the lateral directions. Solid non-slip wall with prescribed heat flux was used at the bottom. Constant temperature and pressure were specified at the top boundaries. These macroscopic boundaries were implemented in mesoscopic level through the use of distribution functions.

The non-slip wall at the bottom and the temperature (heat flux) boundaries were implemented using the method proposed by Inamuro et al. [22]. The pressure at the top has been kept

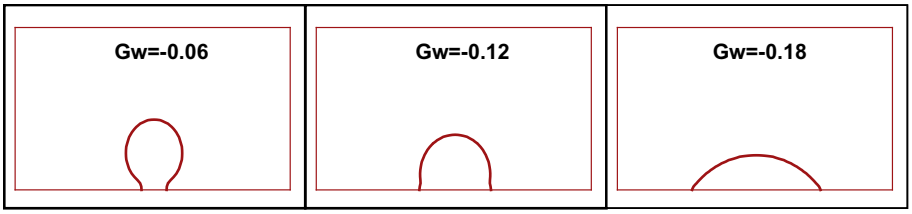

Fig. 3. Contact angles for various liquid–solid interaction strength G_w.

constant using the method of Zhou and He [48]. Finally, we note that the implementation of periodic boundaries is straightforward in LBM.

3. Simulation results

Our numerical boiling simulations were carried out in a rectangular domain. The initial density and temperature fields corresponded to the saturation pressure specified at the top boundary. A density dependent constant body force was used to represent the gravity. For the simulation of slow horizontal flow, a constant body force was applied in the horizontal direction, too. The initial temperature was chosen to be $T = 0.8$ and the contact angle was 30° unless otherwise is specified. The corresponding surface tension can be seen in Fig. 2.

A constant heat flux was applied on the bottom plate with a high flux core at the center. This core represents a cavity with large surface and accordingly larger heat source than its surrounding. It is worth noting that we do not have an initial nucleus at the beginning of the simulations, thus the flux at the center must be high enough to produce the first bubble. Due to the heat flux a bubble starts to grow at the center and thermal boundary develops by heat diffusion adjacent to the wall. When the bubble diameter achieves its departure diameter it detaches from the wall.

The detached bubble is not necessarily a stable object. If its size is smaller than the critical bubble radius then the bubble rises up and its diameter decreases (condenses down) [42]. A possible final state is that the bubble disappears before reaching the upper boundary. On the other hand, bubbles large enough after detachment can reach the upper boundary.

3.1. Finite domain size effect

Preliminary calculations have been performed varying the size of the simulation domain. Since our domain is periodic in the horizontal direction, therefore lateral interactions between bubbles are expected to influence the bubble growing and detachment process. Having sufficiently large domain, these interactions become negligible and the detachment process can be considered as the one of an individual bubble. Fig. 4 shows simulation results obtained in two different domain sizes (150×300 and 300×600) and at various timesteps. For both simulations, the same heat flux profile has been applied at the bottom boundary. Obviously, the domain size does not influence on the bubble growing and detachment process, but it has an effect on the bubble rise. This is due to the effect of the pressure boundary at the top, rather than the lateral hindering between rising bubbles. Decreasing the gravity force, bubbles grow up to larger volumes and lateral interactions can become more relevant. We have found no differences in the bubble growing and detachment processes, when the bubble diameter did not exceed the half of their distance i.e. $D_h < 75$ in a box size 150×300. So results presented in this work for stagnant fluid were obtained at this resolution.

In case of horizontal fluid flow, we doubled (300×300) the lateral domain size in order to reduce lateral cooperation between detached bubbles.

3.2. Heterogeneous boiling in stagnant liquid

Fig. 5 shows a sequence of snapshots of the bubble contour obtained from simulation results by setting the dimensionless gravity

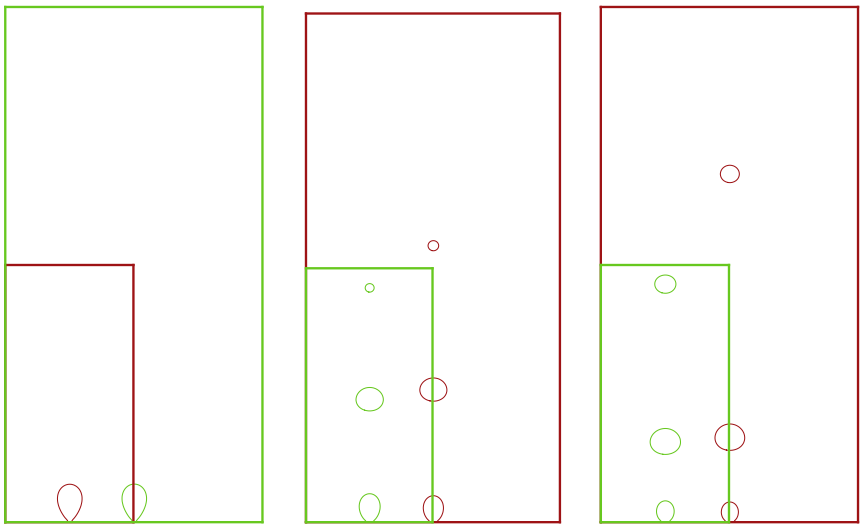

Fig. 4. Domain size effect. Using two different resolutions (150×300 and 300×600) no significant differences can be observed in the bubble detachment process. However, the bubble rise is influenced by the pressure boundary at the top (left – time = 10,000, center – time = 25,000, and right – time = 40,000).

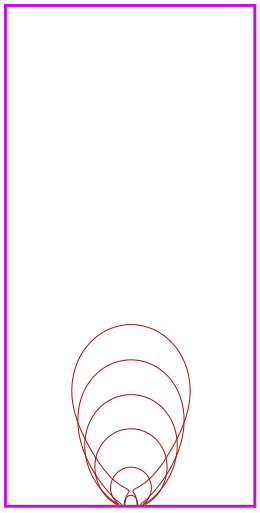

Fig. 5. Shapes of a bubble during growing.

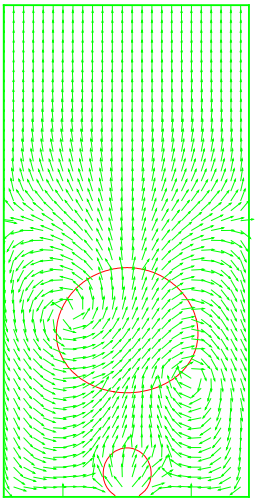

Fig. 7. Velocity field after detachment of the bubble.

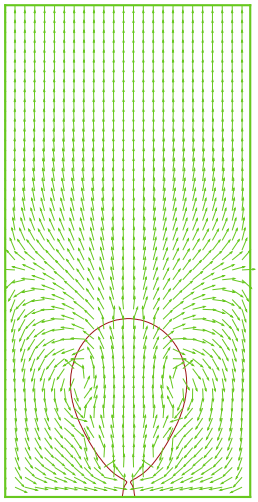

Fig. 6. Velocity field just before detachment of the bubble.

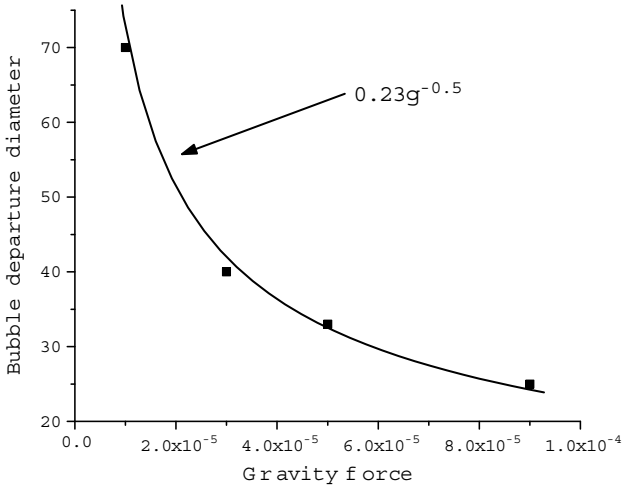

Fig. 8. Departure diameter as a function of gravity.

to $g = 3 \times 10^{-5}$. As one can see, first a small nucleus develops at the high heat flux core. Then the bubble starts to grow and the dry spot increases. Achieving a maximum, the dry spot decreases and finally a bubble neck is formed just before detachment. This neck is important. After detachment, a tiny attached bubble remains on the wall, turning the nucleation into a "heterogeneous" one.

In Figs. 6 and 7 the velocity fields with uniform vector length are shown before and after detachment of the bubble, respectively. Flow circulation can be observed on both sides of the bubble. These circulations transfer cold liquid to the bubble neck clearly supporting the transient micro-convection model proposed by Haider and Webb [15]. The liquid in the wake of the departing bubble induces eddies, which impose a combination of front and inverted stagnation flows of liquid on the surface. As a consequence of these processes unsteady laminar forced-convection heat transfer develops from the nucleation site, which should be taken into account in heat transfer calculations.

It is worth noting that the circulation is asymmetric after detachment, an observation which needs explanation in the future.

3.2.1. Diameter of the bubble at departure

From the simulation results we can determine the diameter of the bubble at departure. Although from static force balance one can expect that the bubble departure diameter D_b satisfies the following relation:

$$D_b \sim \sqrt{\frac{\sigma}{g(\rho_l - \rho_g)}}, \tag{21}$$

as Dhir's review [9] calls our attention, correlations having exponents $g^{-1/3}$ also appear in the literature. Furthermore, the discussion of Buyevich and Webbon [4] casts further doubts on the use of a simple static force balance for bubble departure. It is also worth mentioning that some recent developments basically takes out the gravity from the puzzle and propose correlations without including the gravity explicitly (see e.g. [45,25]).

Using our model we were able to systematically study the effect of gravity on the bubble departure diameter. Varying the gravity force, simulations were performed and the bubble departure diameter was determined.

In Fig. 8 one can see the departure diameter as a function of the gravity force. The symbols represent the simulation results and the solid line is shown to demonstrate that the bubble diameter is proportional to $g^{-1/2}$ in our simulations.

Bubble diameter is sometimes correlated with the contact angle [12], too. To study this feature we varied the parameter of the interaction potential G_w between the solid and fluid and performed

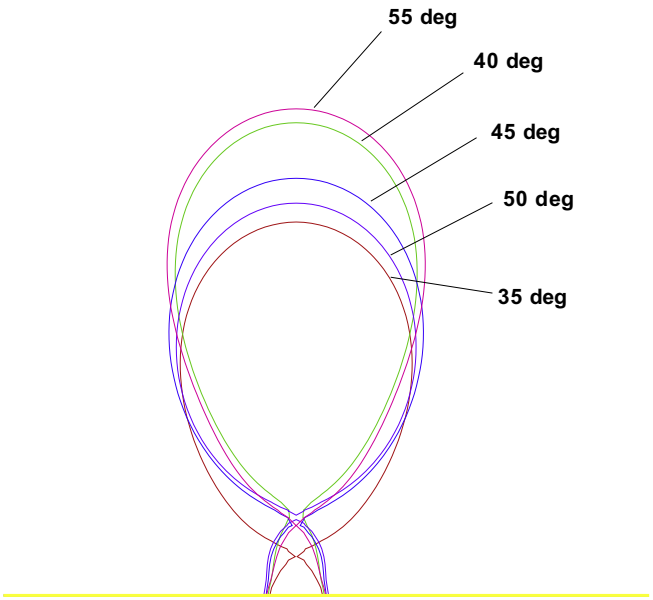

Fig. 9. Departure diameter as a function of the contact angle.

simulations, in order to point out the relation between the bubble departure diameter and contact angle. In Fig. 9 the bubble shapes are shown just before detachment in case of various contact angles. One can see that the bubble diameter is only slightly depends on the contact angle and more importantly no general tendency can be observed between the departure diameter and the contact angle.

On the other hand, we could observe the speed up of the bubble growing with increasing contact angle. Note that these observations contradict some earlier numerical simulations [9] and accordingly, further efforts are needed to explain the observed discrepancies (see next section).

3.2.2. Bubble release frequency

The bubble detachment process is quasi-periodic. Since in our simulations the first bubble does not develop from a nucleus it needs more time to achieve the departure diameter than bubbles grow up later. After detachment of the first bubble a small nucleus remains attached at the bottom wall. The first bubble drags and transfers hot liquid to the bulk changing its temperature. Having the nucleus at the wall and enhanced temperature in the bulk, the development of the second bubble is more rapid than that of the first one. After detachment of the second bubble, a nucleus remains at the bottom wall initiating again a new growing and detachment cycle. Since we apply a constant heat flux at the bottom plate, therefore the temperature is changing continuously in the domain. However, some bubble cycles can be produced without significant changes in the growing and detachment process, therefore the bubble release frequency can be estimated. For instance, in Fig. 10 we show several bubble cycles including the first cycle. These snapshots were taken at 7000, 12,000, 17,000, 22,000, 27,000 and 32,000 simulations steps, so after the first cycle the bubble growth time is periodic with 5000 simulation steps. It is also worth mentioning that the detached bubbles behave slightly differently in the bulk due to the axial change in the temperature profile.

The bubble release frequency f is usually calculated from the correlation proposed by Zuber [49]

$$f^{-1} \sim D_b \left[\frac{\sigma g(\rho_l - \rho_g)}{\rho_l^2}\right]^{-1/4}.$$

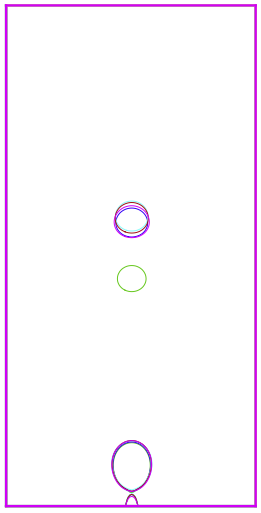

Fig. 10. Periodicity of bubble detachment. Snapshots were taken at 7000, 12,000, 17,000, 22,000, 27,000 and 32,000 simulation steps.

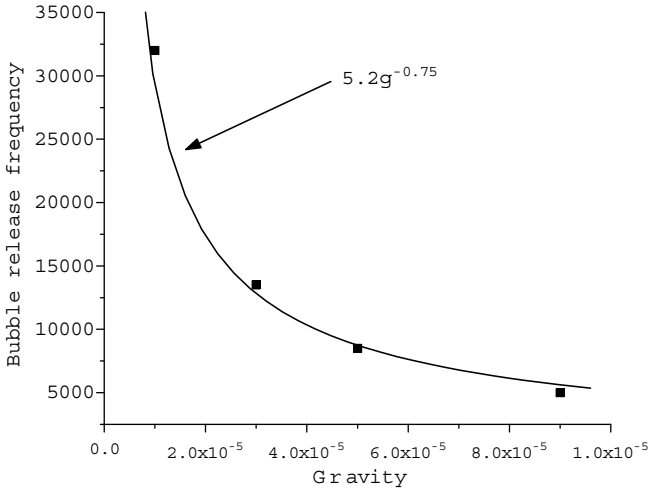

Fig. 11. Bubble release period as a function of gravity.

Knowing the fact that the departure diameter is correlated with the gravity force as $g^{-1/2}$, it is expected that the bubble release frequency is proportional to $g^{3/4}$. Varying the gravity, we determined the relation between the gravity force and the inverse of the release frequency. In Fig. 11 symbols show the simulation results and the solid line represents a function $5.2g^{-3/4}$. Clearly, the bubble release period is proportional to $g^{3/4}$ as it is expected.

As we have mentioned in the previous section, the increase of the contact angle results in more rapid growing of bubbles. In Fig. 12 we show the bubble release period as a function of the contact angle for a given gravity. The symbols represent simulation results, while the solid line is an exponential fit to drive the eye. So, the bubble release frequency increases exponentially with the contact angle.

This observation can be explained by taking also into account that the bubble departure diameter is not a function of the static contact angle, so the growing and departure process do not change qualitatively but they take place in another timescale. Larger contact angle means larger attractive forces between the fluid and the wall. Stronger interaction increases the residence time of the liquid layer adjacent to the wall. Since phase transition speeds up with

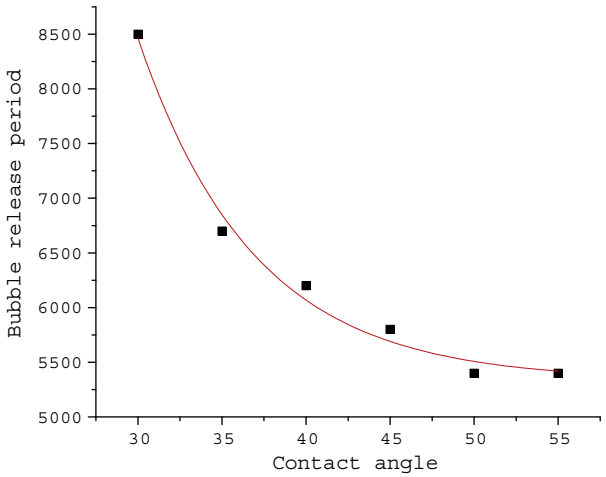

Fig. 12. Bubble release period as a function of the contact angle.

overheating, so the net effect of larger surface tension can be faster growing up of bubbles. It is also worth noting that larger attractive forces support the rewetting of the dry spot, which can give further acceleration to the bubble cycles.

3.3. Heterogeneous boiling in slow flow

Simulations of heterogeneous boiling were carried out accelerating the liquid in the horizontal direction. Using various lateral forces we determined the bubble departure diameter as a function of the applied lateral force.

Fig. 13 shows the shapes of the bubble as it develops in time. At the beginning of the process a small nucleus is formed like in case of the stagnant fluid. Then the bubble starts to grow. During growing, there is obviously a difference between the upstream and downstream contact angles, just like in the measurements of Kandlikar and Stumm [23]. Before detachment a bubble neck appears similarly to the simulations presented in the stagnant fluid.

The velocity vector field with uniform length is shown in Fig. 14 before detachment of the bubble. The plot shows that cold water flows towards the downstream part of the bubble neck, which then be dragged by the bubble and transferred to the bulk. On the other side a circulation zone is formed which gives rise again forced convection heat transfer from the wall. After detachment (Fig. 15) the bubble moves towards the top and similarly to stagnant simulations (Fig. 7), circulation zones develop on both sides of the bubble. Due to the drag of this bubble the cold liquid from the bulk does not reach anymore the downstream part of the second bubble. Rather, it flows towards the bubble dome slowing down its growing.

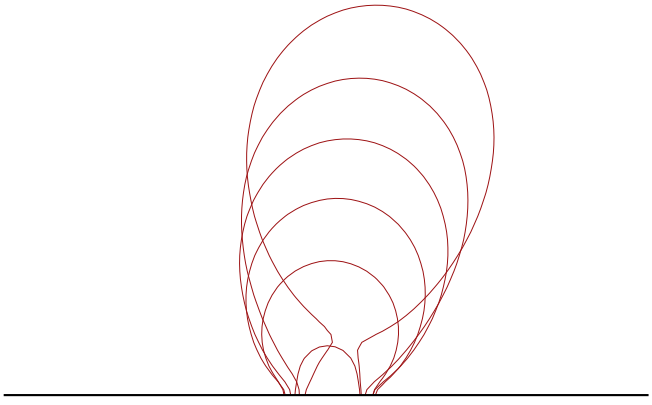

Fig. 13. Bubble shapes in a horizontal background flow.

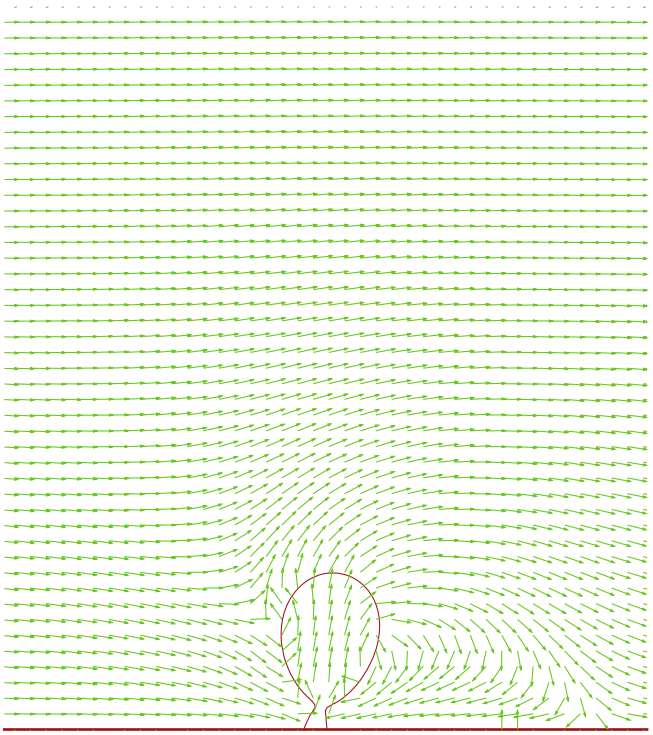

Fig. 14. Velocity vector field before detachment.

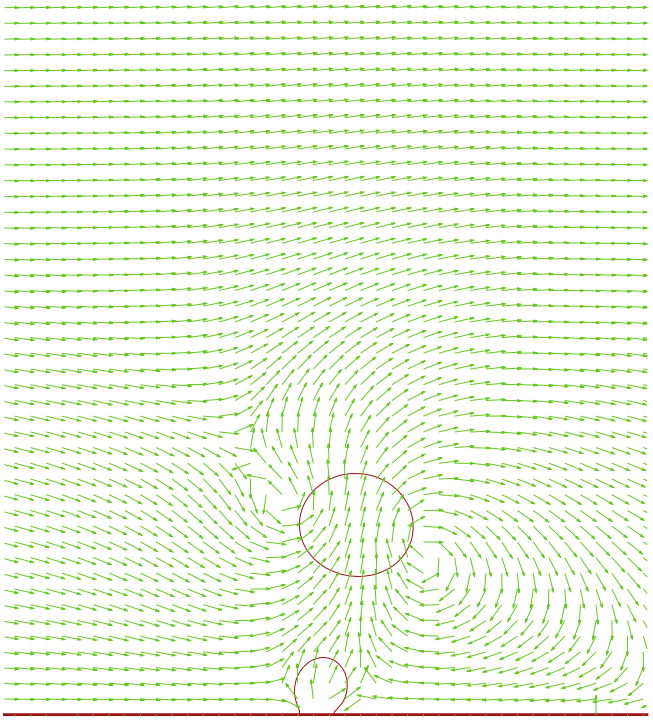

Fig. 15. Periodicity in case of forced flow.

3.3.1. Diameter of the bubble at departure

Increasing the lateral force, we found that the bubble departure diameter decreased exponentially as it can be seen in Fig. 16. This

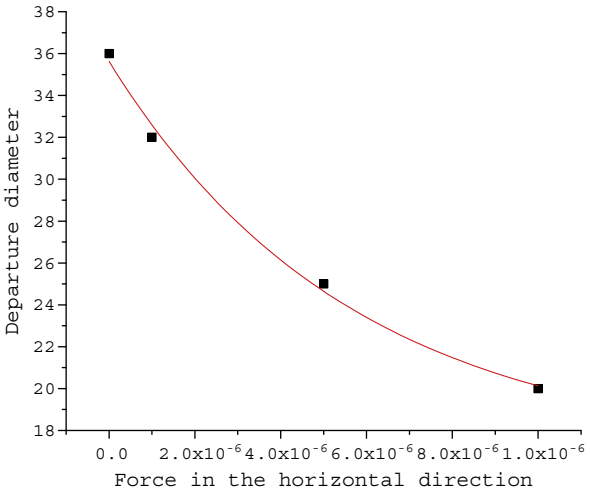

Fig. 16. Bubble departure diameter as a function of the lateral force.

observation is in line with the measurement data presented in [20]. The speed up of bubble detachment is due to a combined effect of various forces acting on the bubble in this situation.

4. Conclusion

Numerical simulation of heterogeneous boiling has been presented using the lattice Boltzmann method. Simulation results demonstrated that the bubble departure diameter and bubble release frequency are proportional to $g^{-1/2}$ and $g^{3/4}$, respectively, where g is the gravitational acceleration. In contrast with some results obtained by others we found no static contact line dependence of the bubble departure diameter. On the other hand, the bubble release frequency has shown exponential decay with the static contact angle. This observation is explained by the speed up of the rewetting process of the dry spot and the increased residence time of the liquid layer adjacent to the wall. Both effects are consequences of the fact that an increase in the static contact angle is due to increasing molecular attractive forces.

Considering heterogeneous forced boiling, the development of upstream and downstream contact angles have been demonstrated. Simulation results shown that the bubble departure diameter decreases exponentially with increasing background flow in line with experimental observations.

Acknowledgement

This work has been supported by the European Integrated Project NURESIM in the sixth framework program of the European Union.

Appendix A. Derivation of the energy equation

Here we derive the form of the energy equation (16) used in this work. Neglecting viscous dissipation the entropy balance equation reads

$$\rho T \frac{\mathrm{d}s}{\mathrm{d}t} = \nabla(k\nabla T). \tag{22}$$

Using the thermodynamic relation

$$T\,\mathrm{d}s = c_\mathrm{v}\,\mathrm{d}T + T\left(\frac{\partial p}{\partial T}\right)_\mathrm{v}, \quad \mathrm{d} = c_\mathrm{v}\,\mathrm{d}T - T\frac{1}{\rho^2}\left(\frac{\partial p}{\partial T}\right)_\rho \mathrm{d}\rho,$$

and substituting it into the entropy balance equation we obtain

$$\rho c_\mathrm{v}\frac{\mathrm{d}T}{\mathrm{d}t} = \nabla(k\nabla T) + \rho T\frac{1}{\rho^2}\left(\frac{\partial p}{\partial T}\right)_\rho \frac{\mathrm{d}\rho}{\mathrm{d}t}.$$

Now, the term (18) is obtained by taking the derivative of the pressure (12) at constant density respect to T.

References

[1] D.K. Agarwal, S.W.J. Welch, G. Biswas, F. Durst, Planar simulation of bubble growth in film boiling in near critical water using a variant of the VOF method, J. Heat Transfer 126 (2004) 329.
[2] P. Arlabosse, L. Tadrist, H. Tadrist, J. Pantaloni, Experimental analysis of the heat transfer induced by thermocapillary convection around a bubble, Trans. ASME 122 (2000) 66.
[3] D. Bestion, H. Anglart, P. Peteraud, B. Smith, E. Krepper, F. Moretti, J. Macek, Review of available data for validation of NURESIM two-phase CFD software applied to CHF investigations, Science and Technology of Nuclear Installations (2008), in press.
[4] Y.A. Buyevich, B.W. Werbon, Dynamics of vapour bubbles in nucleate boiling, Int. J. Heat Mass Transfer 39 (1996) 2409.
[5] H. Chen, S. Chen, W.H. Matthaeus, Recovery of the Navier–Stokes equations using a lattice-gas Boltzmann method, Phys. Rev. E, 45 (1992) R5339.
[6] A.K. Chester, An analytical solution for the profile and volume of a small drop or bubble symmetrical about a vertical axis, J. Fluid Mech. 81 (1977) 609.
[7] J. Chin, P.V. Coveney, Lattice Boltzmann study of spinodal decomposition in two dimensions, Phys. Rev. E 66 (2002) 016303.
[8] S. DasGupta, I.Y. Kim, P.C. Wayner Jr., Use of the Kelvin–Clapeyron equation to model an evaporating curved microfilm, J. Heat Transfer 116 (1994) 1007.
[9] V.K. Dhir, Mechanistic prediction of nucleate boiling heat transfer – achievable or a hopeless task?, J Heat Transfer 128 (2006) 1.
[10] V.K. Dhir, Numerical simulation of pool boiling heat transfer, AIChE J. 47 (2001) 813.
[11] V.K. Dhir, Numerical simulations of pool boiling heat transfer, AIChE J. 47 (2001) 813.
[12] W. Fritz, Berechnung des Maximalvolumens von Dampfblasen, Phys. Z. 36 (1935) 379.
[13] T. Fuchs, J. Kern, P. Stephan, A transient nucleate boiling model including microscale effects and wall heat transfer, J. Heat Transfer 128 (2006) 1257.
[14] Z. Guo, M.S. El-Genk, Liquid microlayer evaporation during nucleate boiling on the surface of a flat composite wall, Int. J. Heat Mass Transfer 37 (1994) 1641.
[15] S.I. Haider, R.L. Webb, A transient micro-convection model of nucleate pool boiling, Int. J. Heat Mass Transfer 40 (1997) 3675.
[16] G. Hazi, P. Kavran, On the cubic velocity deviations in lattice Boltzmann methods, J. Phys. A 39 (2006) 3127.
[17] G. Hazi, A. Markus, Consistent lattice Boltzmann methods with pseudo-potential for two-phase flows, Phys. Rev. E (2007), submitted for publication.
[18] G. Hazi, A. Markus, Lattice Boltzmann simulation of boiling in subchannels, in: Proceedings of the 12th International Topical Meeting on Nuclear Reactor Thermal Hydraulics (NURETH-12), Pittsburgh, Pennsylvania, USA, September 30–October 2007, vol. 4, p. 329.
[19] G. Hazi, A. Markus, Modelling heat transfer in supercritical fluid using the lattice Boltzmann method, Phys. Rev. E 77 (2008) 026305.
[20] W.G.J. Helden, C.W.M. Geld, P.G.M. Boot, Forces on bubbles growing and detaching in flow along a vertical wall, Int. J. Heat Mass Transfer 38 (1995) 2075.
[21] T. Inamuro, T. Ogata, F. Ogino, Numerical simulation of bubble flows by the lattice Boltzmann method, Future Gener. Comput. Syst. 20 (2004) 959.
[22] T. Inamuro, T. Ogata, S. Tajima, N. Konishi, A lattice Boltzmann method for incompressible two-phase flows with large density differences, J. Comput. Phys. 198 (2004) 628.
[23] S.G. Kandlikar, B.J. Stumm, A control volume approach for investigating forces on a departing bubble under subcooled flow boiling, Trans. ASME 117 (1995) 990.
[24] S.G. Kandlikar, M.E. Steinke, Contact angles and interface behaviour during rapid evaporation of liquid on a heated surface, Int. J. Heat Mass Transfer 45 (2002) 3771.
[25] J. Kim, M.H. Kim, On the departure behaviors of bubble at nucleate pool boiling, Int. J. Multiphase Flow 32 (2006) 1269.
[26] I. Kurtoglu, C.L. Lin, Lattice Boltzmann study of bubble dynamics, Numer. Heat Transfer B 50 (2006) 333.
[27] H.S. Lee, H. Merte Jr., Hemispherical vapor bubble growth in microgravity: experiments and model, Int. J. Heat Mass Transfer 39 (1996) 2449.
[28] R.C. Lee, J.E. Nydahl, Numerical calculation of bubble growth in nucleate boiling from inception through departure, Trans. ASME 111 (1989) 474.
[29] R. Marek, J. Straub, The origin of thermocapillary convection in subcooled nucleate pool boiling, Int. J. Heat Mass Transfer 44 (2001) 619.
[30] N.S. Martys, H. Chen, Simulation of multicomponent fluids in complex three-dimensional geometries by the lattice Boltzmann method, Phys. Rev. E 53 (1996) 743.
[31] R. Mei, W. Chen, J.F. Klausner, Vapor bubble growth in heterogeneous boiling - I. Formulation, Int. J. Heat Mass Transfer 38 (1995) 909.

[32] R. Mei, W. Chen, J.F. Klausner, Vapor bubble growth in heterogeneous boiling – II. Growth rate and thermal fields, Int. J. Heat Mass Transfer 38 (1995) 921.
[33] A. Mukherjee, V.K. Dhir, Study of lateral merger of vapor bubbles during nucleate pool boiling, J. Heat Transfer 126 (2004) 1023.
[34] A. Mukherjee, S.G. Kandlikar, Numerical study of single bubbles with dynamic contact angle during nucleate pool boiling, Int. J. Heat Mass Transfer 50 (2007) 127.
[35] R.S. Qin, Bubble formation in lattice Boltzmann immiscible shear flow, J. Chem. Phys. 126 (2007) 114506.
[36] K. Sankaranarayanan, X. Shan, I.G. Kevrekidis, S. Sundaresan, Analysis of drag and virtual mass forces in bubbly suspensions using an implicit formulation of the lattice Boltzmann method, J. Fluid Mech. 452 (2002) 61.
[37] K. Sankaranarayanan, X. Shan, I.G. Kevrekidis, S. Sundaresan, Bubble flow simulations with the lattice Boltzmann method, Chem. Eng. Sci. 54 (1999) 4817.
[38] X. Shan, H. Chen, Lattice Boltzmann model for simulating flows with multiple phases and components, Phys. Rev. E 47 (1993) 1815.
[39] G. Son, V.K. Dhir, N. Ramanujapu, Dynamics and heat transfer associated with a single bubble during nucleate boiling on a horizontal surface, J. Heat Transfer 121 (1999) 623.
[40] G. Son, N. Ramanujapu, V.K. Dhir, Numerical simulation of bubble merger process on a single nucleation site during pool nucleate boiling, J. Heat Transfer 124 (2002) 51.
[41] N.S. Srinivas, R. Kumar, Prediction of bubble growth rates and departure volumes in nucleate boiling at isolated sites, Int. J. Heat Mass Transfer 27 (1984) 1403.
[42] M.C. Sukop, D. Or, Lattice Boltzmann method for homogeneous and heterogeneous cavitation, Phys. Rev. E 71 (2005) 046703.
[43] X. Yin, D.L. Koch, R. Verberg, Lattice Boltzmann method for simulating spherical bubbles with no tangential stress boundary conditions, Phys. Rev. E 73 (2006) 026301.
[45] C. Yang, Y. Wu, X. Yuan, C. Ma, Study on bubble dynamics for pool nucleate boiling, Int. J. Heat Mass Transfer 43 (2000) 203.
[46] G.R. Warrier, N. Basu, V.K. Dhir, Interfacial heat transfer during subcooled flow boiling, Int. J. Heat Mass Transfer 45 (2002) 3947.
[47] S.W.J. Welch, Direct simulation of vapor bubble growth, Int. J. Heat Mass Transfer 41 (1998) 1655.
[48] Q. Zhou, X. He, On pressure and velocity boundary condition for the lattice Boltzmann BGK model, Phys. Fluids 9 (1997) 1591.
[49] N. Zuber, Nucleate boiling. The region of isolated bubbles and the similarity with natural convection, Int. J. Heat Mass Transfer 6 (1963) 53.